Cume #395

90 Points Possible; 68 Points ($\simeq 75\%$) is Guaranteed Pass passes below this score are a distinct possibility
Administered: February 14, 2015

Probing The Fermi Bubbles in Ultraviolet Absorption:

A Spectroscopic Signature of the Milky Way's Biconical Nuclear Outflow
Fox, A. J., et al. (2015), ApJ, 799, L7

Please start each question (by number) on a new sheet of paper, write on only one side of the paper, and staple them together in order of question number when finished. Please present your results in the order that the individual questions appear. Also, please do not write anything in the extreme upper left corner (even the problem number) so that the staple does not obscure your work.

- 1. [15 pts] Overview: Write a nine sentence overview of this paper. Be sure you emphasize the central <u>scientific</u> point (i.e., what is the pig picture the authors attempted to demonstrate to the reader). Points are distributed as follows:
 - (a) [5 pts] In three sentences maximum, describe the big picture/astronomical significance of their work, i.e., the broader context for why they published this paper.
 - The flow of gas around galaxies is centrally important to understanding galaxy evolution and metal enrichment of the IGM, and nuclear galactic winds are one of the most important mechanisms for learning about these astronomical problems. The Fermi Bubble observations suggest such a wind emanates from the nuclear region of the Milky Way and the kinematics have not been well characterized to determine if it is truly a wind. The paper provides the data and analysis to investigate and resolve that issue.
 - (b) [5 pts] In three sentences maximum, describe the observational and analysis methods.
 - The authors obtained COS UV absorption line spectra and GBT radio data of the QSO PDS 456, for which the line of sight pierces both the front side and far side of the Fermi Bubble. They determined the velocity structure of several ions and measure their column densities. They examined co-rotation kinematics and then constructed a simple geometric and kinematic model of the wind, generated the distribution of "absorption velocities" from the model, and compared them to the observed data.
 - (c) [5 pts] In three sentences maximum, describe the main conclusion(s) about the properties of this system.
 - They can explain two of the velocity components as originating in a biconical wind for which they favor a momentum driven wind velocity field (ballistic gas projectiles). They deduce that the wind activity in the Galactic center has lasted somewhere between 2.5-4.0 Myr.
- 2. [15 pts] Standards of Rest and Galactic Coordinates:
 - (a) [5 pts] Explain what the Local Standard at Rest (LSR) frame is. If an object has a line of sight $v_{\rm LSR}=0~{\rm km~s^{-1}}$, does it have a zero or non-zero heliocentric velocity? Explain.
 - The LSR is a velocity coordinate system centered on the sun with a direction given by the mean velocity of the stars in the solar neighborhood. Relative to the LSR, the sun has velocity of 20 km s⁻¹ in the direction RA \simeq 18 hrs DEC $= +30^{\circ}$ in B1950 equatorial coordinates. Heliocentric velocity is the line of sight velocity an object has with respect to the sun (after the Earth's rotation and orbital motion is corrected out). An object has a line of sight $v_{\rm LSR} = 0$ km s⁻¹ will have a non-zero heliocentric velocity, unless it is moving exactly perpendicular to the sun's motion with respect to the LSR.

 The direction of sons motion with respect to the LSR.

 And manage $v_{\rm LSR} = v_{\rm LSR}$

- (b) [5 pts] Explain what the Galactic Standard at Rest (GSR) frame is. If an object in the Galactic plane has a velocity equal to the rotation velocity of the Galaxy, does it have a zero or non-zero velocity in the Galactic Standard at Rest? Explain.
 - The GSR is a non-rotating velocity coordinate system centered on the Galactice center. The velocity vectors are often given in spherical coordinates. An object in the plane of the Galaxy that is rotating with the Galaxy has GSR velocity $\mathbf{v} = 0\,\hat{\mathbf{r}} + v_{\rm rot}\,\hat{\boldsymbol{\Phi}} + 0\,\hat{\boldsymbol{\Theta}}$.
- (c) [5 pts] On the provided diagrams of the Milky Way, draw the galactic coordinates clearly indicating the origin of the galactic coordinate system and the cardinal directions $l = 0^{\circ}$, 90° , 180° , and 270° , and $b = 0^{\circ}$ and $b = \pm 90^{\circ}$ with respect to the origin of the system.
 - See the included figure. The origin is the sun. $l=0^{\circ}$ is in the direction of the Galactic center. $l=90^{\circ}$ is in the direction of Galactic rotation. $l=180^{\circ}$ is in the direction of Galactic anti-center. $l=90^{\circ}$ is in the direction opposite of Galactic rotation. $b=0^{\circ}$ is the plane of the galaxy. $b=+90^{\circ}$ is the direction of the north Galactic pole. $b=-90^{\circ}$ is the direction of the south Galactic pole.

3. [25 pts] The Model:

(a) [5 pts] Why do the authors examine the absorption velocities in both the LSR and GSR frames (what do they learn from looking at the data in each frame and what *specific findings* motivate the design of their model)?

First the earth's motion is subtracted out yielding absorption velocities relative to the Sun (heliocentric frame); then the velocities are converted to the LSR to remove the sun's peculiar velocity relative to Galactic rotation at the solar circle. In the LSR, the velocity can be compared to the galactic rotation to examine if the absorbing gas motion is consistent with Galactic rotation. In this paper, they find that some of the gas can be explained as material co-rotating with the Galaxy, but some cannot. Since the authors are investigating winds that are expected to have velocities heading radially out of the Galactic center, they convert the aborption to the GSR in order to examine the gas in terms of outflowing material. They find that the lowest velocity absorbing component is consistent with material coming toward the sun relative to the Galactic center and the highest velocity absorbing component is consistent with material moving away from the sun relative to the Galactic center. This latter result motivates the design of a biconical outflow model to explain these two components (and possibly the gas that is not inconsistent with Galactic rotation).

(b) [5 pts] Describe the model. Include in your answer the design of the model, the three principle free parameters, and all of the other assumptions they have adopted/incorporated.

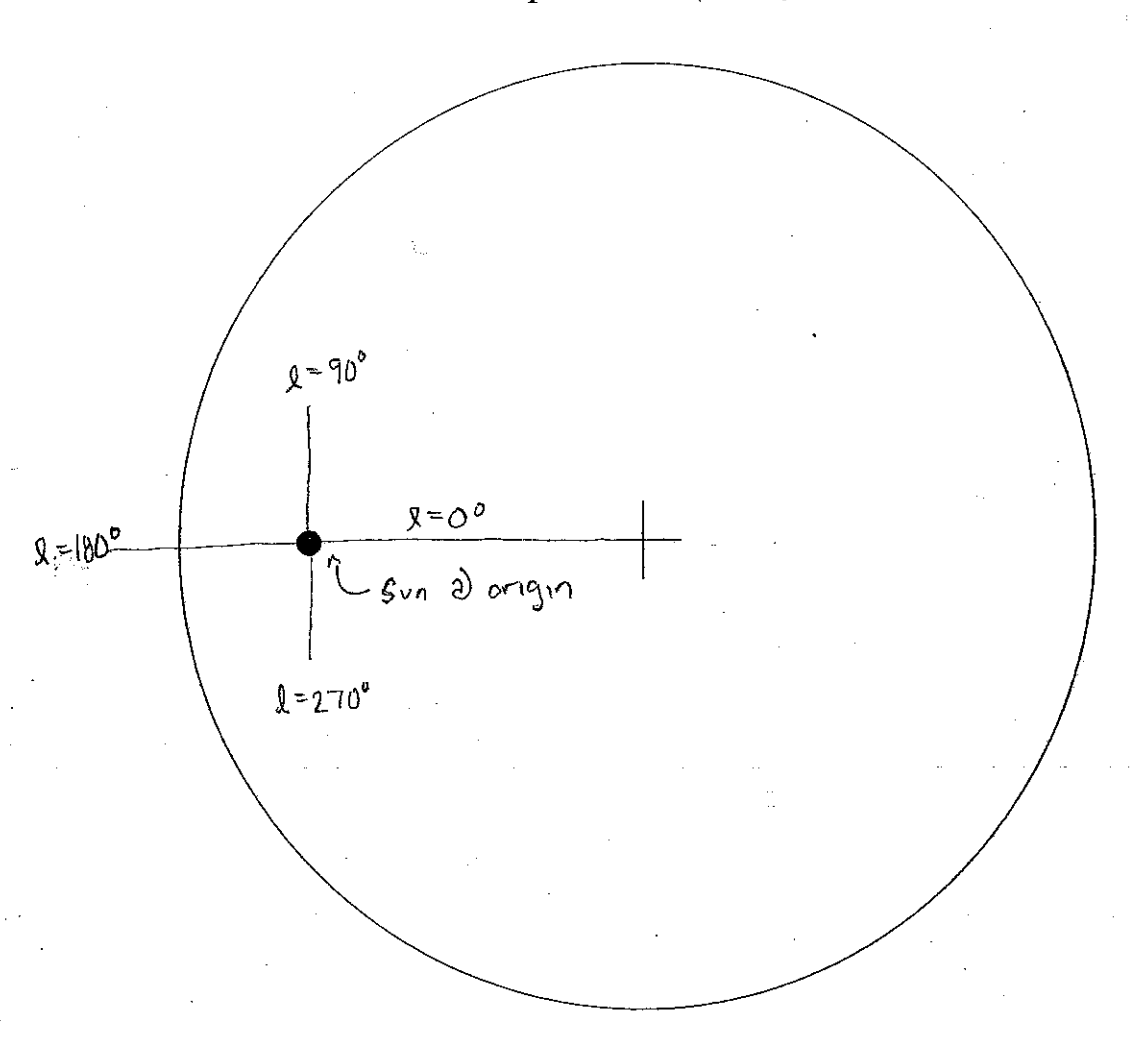
The authors model the absorption kinematics as a biconical outflow from the Galaxy center. The principle free parameters are $v_{\rm out}$, the velocity at the base of the bicone, α , the full opening angle of the bicone, and the velocity profile. They explore two velocity profiles, constant velocity and momentum-driven (velocity slows as it climbs ballistically out of the gravitational potential; they call this momentum-driven because the velocity at the base is assumed to result from an impulse from ram pressure from the hot wind). They assume (1) a non-rotating radial outflow confined in the bicone with (2) constant mass flux, (3) uniform filling factor, and (4) a flow populated with 10^7 test particles.

(c) [5 pts] What are the experimental constraints placed on their model? Which version of the model do they adopt and why?

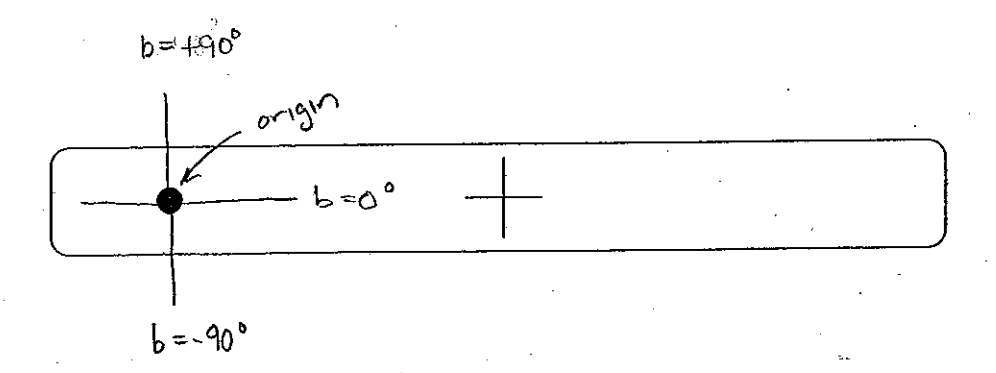
The line of sight must pierce the wind model, which requires the model extent up to 4 kpc above the Galactic disk. They adopt $\alpha=110^\circ$ based upon ROSAT 1.5 keV images of the FB. The authors favor (adopt) $v_{\rm out}>900$ km s⁻¹ because smaller $v_{\rm out}$ cannot reproduce

- Galactic center

Top view of Galaxy



Side view of Galaxy



the $-235~\rm km~s^{-1}$ component. They adopt the momentum-driven velocity field model over the constant velocity field model because the constant velocity model predicts substantial absorption on the range 300-600 km s⁻¹, and no such absorption is detected.

- (d) [5 pts] Consider the very bottom panel of Figure 3 in the paper. Draw a version of this figure for a constant velocity model in which the low ionization gas does not have uniform filling factor but is instead assumed to be confined along the surface of the cones of the outflow. In other words, what do you roughly expect would be the averaged outcome of such a model in terms of the velocity distribution? Explain why you drew your velocity distribution the way you did.
 - The key to this question is to examine the two top panels of Figure 3. According to the colored velocity LRS field, the LSR velocities where the cone surfaces are intersected by the line of sight are $\sim -200~\rm km~s^{-1}$ (near side) and $\sim +300~\rm km~s^{-1}$ (far side). So the the bottom panel of Figure 3 would have two very narrow velocity distributions with peaks at $\sim -200~\rm km~s^{-1}$ and $\sim +300~\rm km~s^{-1}$. The width of these peaks would depend upon how thick one assumes the cone walls to be.
- (e) [5 pts] Assuming the authors had adopted such a model as described in part (d), speculate on what variations in the model they would need to explore in order to recover a velocity distribution like the one they show in Figure 3 that successfully explains the data? Do you think that this would have been an effective approach to the modeling? [HINT: there is no single "correct" answer, this question is about your "insights" into doing this kind of science.]
 - Said model cannot explain the components with $v_{\rm LSR}=-5$ and +30 km s⁻¹. So those components could be explained as co-rotating with the Galaxy, which is a plausable explanation. However, additional free parameters could be incorporated to explore said model. Some examples are: (1) explore the thickness of the cone wall; (2) consider a distribution of velocities at the base of the cone (the launch velocity, $v_{\rm out}$); (3) allow for multiple episodes of the outflow each having a different opening angle α . The problem with adding additional free parameters is that (1) fine tuning can likely get you to match the data even with unphysical parameters, and (2) the story or main point of the exercise gets lost in plausible but not important details. Fairly unphysical parameters would likely be required to try and explain the $v_{\rm LSR}=-5$ and +30 km s⁻¹ components as originating in the wind, so it is doubtful that the authors would be successful at explaining all components with said model. So, the authors made a good choice to keep the model simple.

gas derectle.

4. [15 pts] The COS Spectrum:

(a) [5 pts] Given the FWHM of the velocity resolution of the COS spectrum (as stated by the authors), what is the resolution, R, of the spectrum?

The velocity resolution is $\Delta v = 20$ km s⁻¹ (FWHM). The resolution, R, is $R = \lambda/\Delta\lambda$, where $\Delta\lambda$ is the FHWM of a resolution element. From $\Delta\lambda/\lambda = \Delta v/c$, we have $R = c/\Delta v = 300,000/20 = 15,000$.

(b) [5 pts] Given the number of pixels per resolution element of the spectrum (as stated by the authors), what is the dispersion of the spectrum in km s⁻¹ pixel⁻¹?

The velocity resolution is $\Delta v = 20$ km s⁻¹ (FWHM), which is a single resolution element. The number of pixels per resolution element is 7. We have 20/7 = 2.86 km s⁻¹ pixel⁻¹.

- (c) [5 pts] What is the dispersion of the spectrum in \mathring{A} pixel⁻¹ at the midpoint of the covered wavelength interval?
 - From $\Delta\lambda = \lambda/R$, we see that the FWHM of a resolution element in Å changes in linear proportion to λ . The wavelength interval of the spectrum is 1133–1778 Å, with midpoint 1456 Å. We thus have $\Delta\lambda = 1456/15,000 = 0.097$ Å (FHWM). Since there are 7 pixels per resolution element, we have 0.014 Å pixel⁻¹.

- 5. [20 pts] Testing Co-Rotation: You take a spectrum of a QSO in the direction $l=30^{\circ}$ and $b=0^{\circ}$ and measure the line of sight velocity, v_{los} , of an absorption line from a cloud in the Galactic disk. You happen to know that the cloud has a distance of d=12 kpc from the sun, which is $R_{\odot}=8$ kpc from the center of the Galaxy.
 - (a) [5 pts] What is the distance of the cloud, r, from the center of the Galaxy (in kpc)? Partial credit will be given so show your work clearly. A diagram will be very helpful.

See the included diagram. Use the law of cosines: $r^2 = d^2 + R_{\odot}^2 - 2dR_{\odot}\cos l$. We have r = 6.45 kpc.

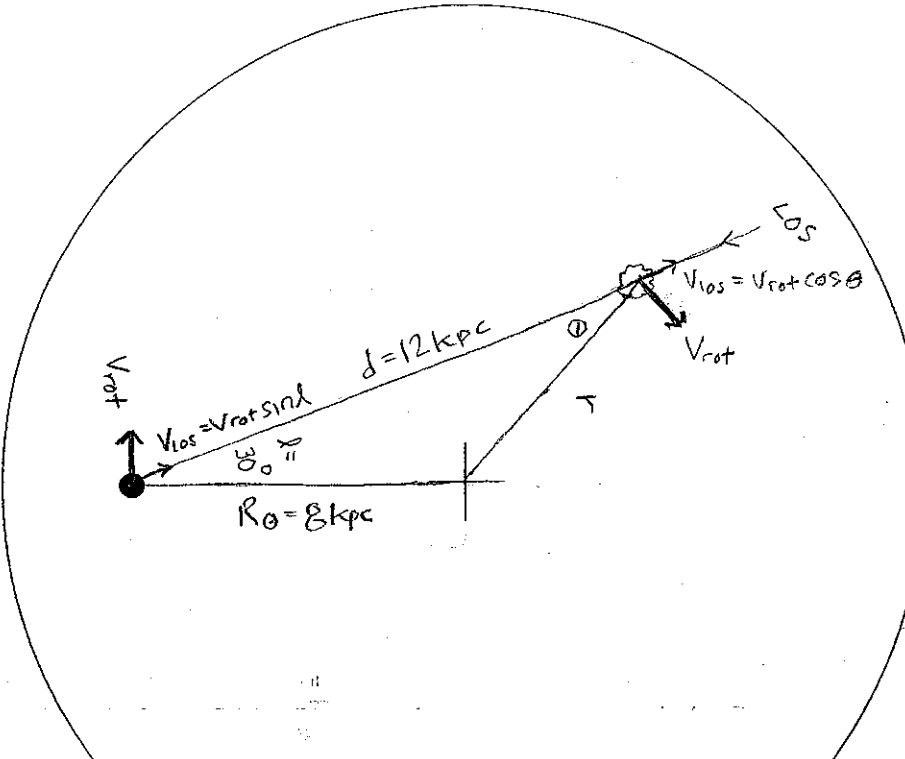
(b) [15 pts] If the rotation velocity of the Galaxy plane is $v_{\rm rot} = 250$ km s⁻¹ at all r, compute the expected line of sight velocity of the cloud (in km s⁻¹) if the sun and the cloud are undergoing circular rotation. Partial credit will be given so show your logic and work clearly. [As with all problems, if you can work out the formula symbolically before plugging in numbers you may find the actual calculation to be substantially simplified. Also, it will be much easier to provide partial credit for your work.]

See the included diagram. The rotation velocity for the sun is in the direction $l=90^\circ$. The line of sight velocity will be the difference between the cloud's and the sun's velocity projections along the line of sight, $v_{\rm los}=v_{\rm los}^{\rm cl}-v_{\rm los}^\odot$. From basic trig, we directly see that $v_{\rm los}^{\rm cl}=v_{\rm ot}\cos\theta$, where θ is the angle opposite the vertex at the sun's location. From the law of sines, $\sin\theta=(R_\odot/r)\sin l$. Thus, $v_{\rm los}^{\rm cl}=v_{\rm rot}\frac{[1-(R_\odot/r)^2\sin^2 l]^{1/2}}{[1-(R_\odot/r)^2\sin^2 l]^{1/2}}$. Evaluating, we have $v_{\rm los}^{\rm cl}=0.78v_{\rm rot}$. O-62. From basic trig, we see that $v_{\rm los}^\odot=v_{\rm rot}\sin l$. Evaluating, we have $v_{\rm los}^{\rm cl}=0.50v_{\rm rot}$. Thus, the line of sight velocity of the cloud is $v_{\rm los}=v_{\rm los}^{\rm cl}-v_{\rm los}^\odot=(0.78-0.50)v_{\rm rot}=0.26v_{\rm rot}=0.79v_{\rm rot}=0.26v_{\rm rot}=0.12$

30 km/s

Galactic center

Top view of Galaxy



law of cosines $r^2 = d^2 + R_0^2 - 2dR_0 \cos \theta$ d=12 kpc

Ro = 8KPC

e = 30°

r = 6.45 kpc

distance of cloud from center of the Galaxy

5B SIND SIND RO T SIND = Rosinl

cloud: Vios = Vrot \[1 - \left(\frac{Ro}{r} \right)^2 \sin^2 \left\]

SUN VIOS = Vrot SIN &

you must account for sun's tos velocity!

measured Vlos = Vlos - Vlos

Vios - Vrot { \left[1-\left(\frac{R\alpha}{r}\right)^2 \sin^2 \left[- \sin\left]

Vlos = Vrot & 0.78 - 0.5 }

V105 = 0.28 Vrot = 70 km/s

Side view of Galaxy

PROBING THE FERMI BUBBLES IN ULTRAVIOLET ABSORPTION: A SPECTROSCOPIC SIGNATURE OF THE MILKY WAY'S BICONICAL NUCLEAR OUTFLOW*

Andrew J. Fox¹, Rongmon Bordoloi¹, Blair D. Savage², Felix J. Lockman³, Edward B. Jenkins⁴, Bart P. Wakker², Joss Bland-Hawthorn⁵, Svea Hernandez¹, Tae-Sun Kim⁶,

ROBERT A. BENJAMIN⁷, DAVID V. BOWEN⁴, AND JASON TUMLINSON¹

¹ Space Telescope Science Institute, 3700 San Martin Drive, Baltimore, MD 21218, USA; afox@stsci.edu

² Department of Astronomy, University of Wisconsin-Madison, 475 North Charter Street, Madison, WI 53706, USA

³ National Radio Astronomy Observatory, P.O. Box 2, Rt. 28/92, Green Bank, WV 24944, USA

⁴ Princeton University Observatory, Princeton, NJ 08544, USA

⁵ Institute of Astronomy, School of Physics, University of Sydney, NSW 2006, Australia

⁶ Osservatorio Astronomico di Trieste, Via G.B. Tiepolo 11, I-34143 Trieste, Italy

⁷ Department of Physics, University of Wisconsin-Whitewater, 800 West Main Street, Whitewater, WI 53190, USA

**Received 2014 December 2; accepted 2014 December 18; published 2015 January 19

ABSTRACT

Giant lobes of plasma extend $\approx 55^{\circ}$ above and below the Galactic center, glowing in emission from gamma rays (the Fermi Bubbles) to microwaves and polarized radio waves. We use ultraviolet absorption-line spectra from the Hubble Space Telescope to constrain the velocity of the outflowing gas within these regions, targeting the quasar PDS 456 (ℓ , b = 10.4, +11.2). This sightline passes through a clear biconical structure seen in hard X-ray and gamma-ray emission near the base of the northern Fermi Bubble. We report two high-velocity metal absorption components, at $v_{LSR} = -235$ and +250 km s⁻¹, which cannot be explained by co-rotating gas in the Galactic disk or halo. Their velocities are suggestive of an origin on the front and back side of an expanding biconical outflow emanating from the Galactic center. We develop simple kinematic biconical outflow models that can explain the observed profiles with an outflow velocity of $\gtrsim 900$ km s⁻¹ and a full opening angle of $\approx 110^{\circ}$ (matching the X-ray bicone). This indicates Galactic center activity over the last ≈ 2.5 -4.0 Myr, in line with age estimates of the Fermi Bubbles. The observations illustrate the use of UV spectroscopy to probe the properties of swept-up gas venting into the Fermi Bubbles.

Key words: Galaxy: center - Galaxy: evolution - Galaxy: halo - ISM: jets and outflows - ISM: kinematics and dynamics

1. INTRODUCTION

The nuclei of star-forming galaxies are the powerhouses where super-massive black holes collect interstellar gas from their surroundings, funnel it onto accretion disks, and heat it to extreme temperatures. The energy released from these environments and from supernovae and stellar winds drives gas out of galaxies through large-scale galactic winds (see reviews by Heckman 2002; Veilleux et al. 2005). Many outflows in nearby star-forming galaxies are nuclear in origin and biconical in shape, as in NGC 3079 (Cecil et al. 2001, 2002), M82 (Bland & Tully 1988; Shopbell & Bland-Hawthorn 1998; Ohyama et al. 2002), and NGC 1482 (Veilleux & Rupke 2002).

Our vantage point inside the dusty rotating disk of the Milky Way hampers our knowledge of any Galactic nuclear outflow. Lockman (1984) noted an absence of H1 in the inner Galaxy and suggested it had been cleared out by a wind. The first clear detection of a biconical outflow was made in mid-IR emission and (on larger scales) in hard X-ray emission (Bland-Hawthorn & Cohen 2003). It has since become clear that the Galactic center (GC) lies between two giant, energetic lobes associated with outflowing gas. These lobes extend $\approx 55^{\circ}$ above and below the GC (≈ 12 kpc) and show enhanced emission across the electromagnetic spectrum, including: (1) γ -ray

emission, i.e., the Fermi Bubbles (FBs; Su et al. 2010; Dobler et al. 2010; Ackermann et al. 2014), (2) soft X-ray emission at their base (0.3–1.0 keV; Snowden et al. 1997; Kataoka et al. 2013), (3) K-band microwave emission (23–94 GHz), known as the so-called Wilkinson Microwave Anisotropy Probe haze (Finkbeiner 2004; Dobler & Finkbeiner 2008), and (4) polarized radio emission at 2.3 GHz (synchrotron radiation; Carretti et al. 2013). Near the base of the FBs, within 700 pc of the GC, McClure-Griffiths et al. (2013, hereafter MG13) recently discovered a population of \approx 100 small H I clouds whose kinematics are consistent with a biconical outflow with a velocity of \approx 200 km s⁻¹.

Clearly, a nuclear outflow is being driven out from the GC. Yet only a handful of GC sightlines have published UV spectroscopy that constrains the kinematics, ionization state, and elemental abundances of the nuclear outflow, including two active galactic nucleus (AGN) directions (Keeney et al. 2006) and several stellar directions (Bowen et al. 2008; Zech et al. 2008; Wakker et al. 2012). However, none of these UV studies have probed a full sightline through the front and back sides of the FBs within 20° of the GC, where the γ -ray emission, X-ray emission, and (presumably) wind activity is strongest. The only such sightline with published data is the *optical* spectrum of the blue supergiant LS 4825 (ℓ , $b = 1.7, -6.6, d = 21 \pm 5$ kpc), which shows complex multi-component Ca II and Na I profiles spanning \approx 300 km s⁻¹ (Ryans et al. 1997).

We have initiated an observing program with the *Hubble Space Telescope (HST)* to study the gas in the GC region (defined here as $0^{\circ} < l < 30^{\circ}$ and $330^{\circ} < l < 360^{\circ}$) with UV spectroscopy (Program IDs 12936 and 13448). The quasar

^{*} Based on observations taken under program 13448 of the NASA/ESA Hubble Space Telescope, obtained at the Space Telescope Science Institute, which is operated by the Association of Universities for Research in Astronomy, Inc., under NASA contract NAS 5-26555, and under program 14B-299 of the NRAO Green Bank Telescope, which is a facility of the National Science Foundation operated under cooperative agreement by Associated Universities, Inc.

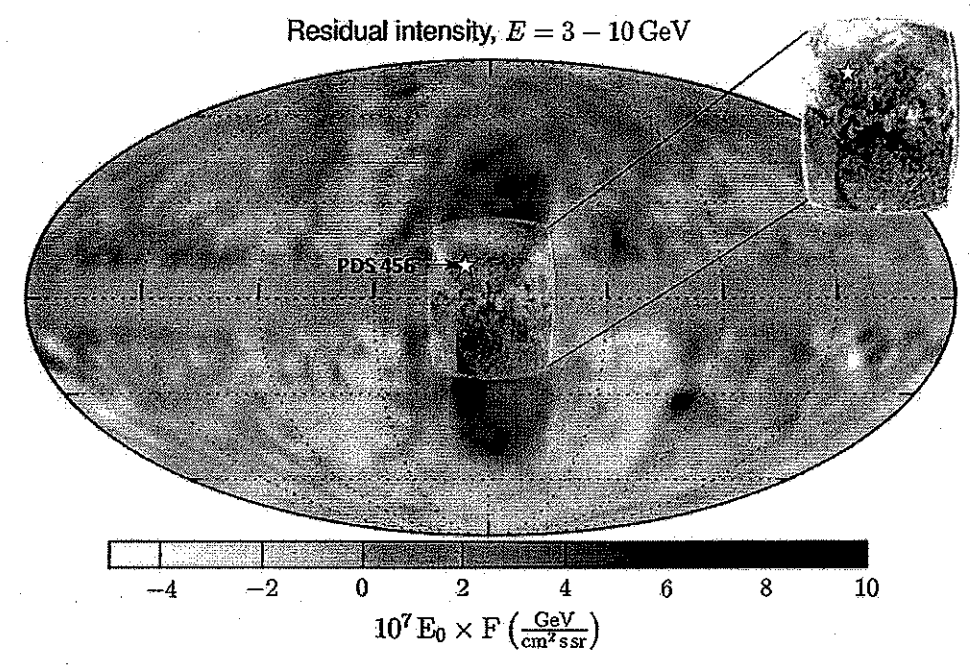


Figure 1. Collage of gamma-ray and X-ray emission showing the striking biconical nuclear structure intercepted by the PDS 456 sightline. The yellow/orange map is an all-sky *Fermi* image of the residual gamma-ray intensity in the 3-10 GeV range, in Galactic coordinates centered on the GC (reproduced with permission from Ackermann et al. 2014). The Fermi Bubbles are the twin lobes in dark orange at the center of the figure. Superimposed in gray-scale is the *ROSAT* diffuse 1.5 keV emission map, based on Snowden et al. (1997), Blānd-Hawthorn & Cohen (2003), and Veilleux et al. (2005). The inset on the right shows a zoom-in on the X-ray data. Adapted from Figure 22, Ackermann et al. (2014).

PDS 456 ($z_{em} = 0.184$, ℓ , b = 10.4,+11.2, also known as IRAS 17254-1413) has the lowest latitude and smallest impact parameter to the GC ($\rho = 2.3$ kpc) of any AGN in our sample. Furthermore, this sightline is the only AGN direction in our sample that passes through the biconical region of enhanced ROSAT 1.5 keV X-ray emission centered on the GC (Snowden et al. 1997), where the γ -ray emission is also strong since the direction intersects the base of the northern FB (Su et al. 2010). The PDS 456 direction (see Figure 1) is therefore of high interest for looking for UV outflow signatures. There are no known 21 cm (neutral) high-velocity clouds (HVCs) in this direction (e.g., Putman et al. 2012).

In this Letter we present new UV and radio spectra of PDS 456 to explore the properties of gas entrained in the Galactic nuclear outflow. In Section 2 we discuss the observations and their reduction. In Section 3 we present the UV absorption-line spectra and discuss the identification of outflow components. Motivated by the component structure observed in our spectra, we present numerical kinematic models of a nuclear biconical outflow in Section 4. In Section 5 we present a discussion of our results. A full discussion of other directions that penetrate the northern and southern FBs will be presented in an upcoming paper.

2. OBSERVATIONS AND DATA REDUCTION

2.1. COS Spectra

PDS 456 was observed on 2014 February 10 with the Cosmic Origins Spectrograph (COS; Green et al. 2012) on board HST for a total of five orbits. The observations used the G130M/1291 and G160M/1600 grating/central wavelength settings, all four FP-POS positions, and exposure times of 4846 s for G130M and 8664 s for G160M. Individual exposures were aligned in velocity space using the centroids of known low-

ion interstellar absorption lines, and then co-added following the same procedures as described in Fox et al. (2014). The spectra have a velocity resolution (FWHM) of ≈20 km s⁻¹, a signal-to-noise ratio near the absorption lines of interest of ≈12–20 (per resolution element), an absolute velocity scale uncertainty of ≈5 km s⁻¹, and cover the wavelength interval 1133–1778 Å, with small gaps between detector segments at 1279–1288 and 1587–1598 Å. The spectra were normalized around each absorption line using linear continua and for display are rebinned by seven pixels (one resolution element), though the Voigt-profile fits (described below) were made on the unbinned data.

2.2. GBT Spectra

We obtained several deep H 1 21 cm pointings of the PDS 456 direction using the Green Bank Telescope (GBT) under NRAO program GBT/14B-299, with the goal of detecting the HV components in emission. Multiple scans of PDS 456 were taken on 2014 October 3 and 4 with the VEGAS spectrometer in frequency-switching mode, for a total of 35 minutes of integration. The data were taken by frequency-switching either 3.6 or 4.0 MHz, resulting in an unconfused velocity range of at least 760 km s⁻¹ about zero velocity at an intrinsic channel spacing of 0.151 km s⁻¹. The spectra were Hanning smoothed, then calibrated and corrected for stray radiation using the procedure described by Boothroyd et al. (2011). One of the receiver's two linear polarizations (PLNUM = 1) gave consistently superior instrumental baselines so only those data were used. A fourthorder polynomial was removed from emission-free portions of the final average. The resulting spectrum has an rms brightness temperature noise of 17.5 mK in a 0.30 km s⁻¹ channel, giving a 1 σ sensitivity to a line 40 km s⁻¹ wide (chosen to be typical of Galactic HVCs) of $N(H I) = 1.1 \times 10^{17} \text{ cm}^{-2}$.

Table 1
Column Densities in the Metal Absorption Components toward PDS 456^a

v _{LSR} (km s ⁻¹)	log <i>N</i> (Si п)	log N (Si nı)	log N (Si rv)	log N (CII)	log <i>N</i> (C1v)	log N (N v)	log N(C1v)/N(Si1v)
-235	13.02 ± 0.08	13.13 ± 0.05	12.90 ± 0.06	13.80 ± 0.14	13.79 ± 0.05	• • • •	0.89 ± 0.07
-5 ^b	14.76 ± 0.05	>14.04	14.05 ± 0.05		14.71 ± 0.05	14.09 ± 0.05	0.66 ± 0.05
+130 ^b	13.40 ± 0.05	13.06 ± 0.05	13.03 ± 0.16	14.14 ± 0.12	13.58 ± 0.06	•••	0.55 ± 0.17
+250	13.37 ± 0.05	12.85 ± 0.05	• • •		•••	•••	

Notes.

3. IDENTIFICATION OF OUTFLOW COMPONENTS

The COS spectra of PDS 456 show four absorption components (see Figure 2), centered at $v_{LSR} = -235, -5, +130$, and +250 km s⁻¹. Absorption is seen in low-ionization (C II, Si II, Al II), intermediate-ionization (Si III), and high-ionization (C IV, Si IV, N V) species, though the relative strength of absorption differs between components. The -235, -5, and +130 km s⁻¹ components show absorption in the low, intermediate, and high ions, whereas the +250 km s⁻¹ component is seen in the lowand intermediate ions only (no CIV, SiIV, or NV). HI emission in the GBT spectrum is only seen in the -5 km s^{-1} component; in the other three components no H1 detection is made down to a sensitive 3σ upper limit $N(H_1) < 3.3 \times 10^{17}$ cm⁻². The ionic column densities in the absorption components are given in Table 1. These were determined by fitting Voigt profiles to the data with the VPFIT software, 8 using simultaneous fits to all available lines of a given ion.

Foreground gas in the rotating disk of the Galaxy produces absorption at a range of LSR velocities, and a simple model of Galactic rotation can be used to predict the maximal allowed velocities for a given latitude and longitude (e.g., Savage & Massa 1987), assuming cylindrical co-rotation. Absorption detected *outside* this velocity interval can be attributed to inflow or outflow. Toward PDS 456 the minimum and maximum LSR velocities are $\approx 0 \text{ km s}^{-1}$ (at a distance of 0.0 kpc) and $+174 \text{ km s}^{-1}$ (at 8.8 kpc), respectively. Therefore:

- The strong -5 km s⁻¹ component can be (either partially or completely) explained by foreground gas in the Galactic disk.
- 2. The +130 km s⁻¹ component corresponds to distances of 7.1 and 9.9 kpc for co-rotation and so could also be tracing Galactic material at z-distances of 1.4 and 1.9 kpc, respectively. However, for distant inner Galaxy sightlines, the assumption of co-rotation breaks down at |z| > 1 kpc (Savage et al. 1990; Sembach et al. 1991), potentially because the gas has been cleared out by a wind. Thus the +130 km s⁻¹ component might trace a nuclear outflow, but we cannot conclusively determine its origin.
- 3. The -235 and +250 km s⁻¹ components are at least 235 and 76 km s⁻¹ away from co-rotation, respectively, and are therefore of most interest for a nuclear outflow. In the galactic standard of rest (GSR), their velocities are -190 and +295 km s⁻¹, assuming the rotation velocity at the solar circle is +254 km s⁻¹ (Reid et al. 2009), and where $v_{\rm GSR} = v_{\rm LSR} + 254$ sin ℓ cos b. The velocities of these two components are consistent with an origin on the front (approaching) and back (receding) sides of a biconical

nuclear outflow emanating from the GC, a scenario modeled in Section 4 and discussed in Section 5.

We note that the observed low-velocity high-ion absorption (CIV, SiIV, and NV) is strong compared to other (non-GC) Galactic halo sight lines (Savage et al. 2001; Wakker et al. 2012). In particular, CIV shows a ≈0.5 dex excess in low-velocity column density, which may be another sign of GC activity.

4. BICONICAL OUTFLOW NUMERICAL MODELS

We develop simple numerical models to explore the kinematic predictions of a biconical nuclear outflow. The models are based on the Mg II outflow models of Bordoloi et al. (2014). We assume the outflow is a non-rotating expanding bicone centered on the GC with a constant mass flux. A population of 10⁷ test particles is inserted at the base of the outflow, with a uniform filling factor. The three principal free parameters in the models are the initial outflow velocity v_{out} , the full opening angle α of the bicone, and the velocity profile. We take α = 110° based on the bicone seen in the ROSAT 1.5 keV image (Figure 1) and investigate the value of v_{out} needed to explain the -235 and +250 km s⁻¹ components. We explore two cases for the velocity profile: constant-velocity (the simplest case), and momentum-driven, where the outflow climbs ballistically out of the Galactic potential after being given an initial impulse (e.g., by ram pressure from a hot wind). In the latter case we use the formalism of Murray et al. (2005) and Dijkstra & Kramer (2012) to express the velocity as a function of radius from the GC. We assume the outflow reaches a radial distance of at least 4 kpc, distant enough to ensure the PDS 456 sightline fully intercepts the bicone (see Figure 3, middle panel). The models are initially computed in the GSR reference frame, but are transformed into the LSR frame for comparison with the data. For both the constant-velocity and momentum-driven cases, 100 realizations of the models are created, and for each one a lineof-sight with the PDS 456 coordinates was generated and the kinematic structure measured. The models do not account for the physical or kinematic properties of the external gaseous medium that confines the flow.

The models are shown in Figure 3. We find $v_{out} \gtrsim 900 \, \mathrm{km \, s^{-1}}$; lower velocities do not account for the $-235 \, \mathrm{km \, s^{-1}}$ component. Figures 3 (top, top view) and (middle, side view) show the velocity structure of the outflow as observed from vantage points outside the Galaxy. These plots illustrate the correspondence between LSR velocity and distance along the line-of-sight. The velocity fields are asymmetric with respect to the vertical because of the transformation from the GSR to LSR frame, i.e., because we are observing the outflow from a co-rotating frame at a fixed distance. Figure 3 (bottom) shows the distribution

^a Errors are statistical only. No entry is given for blends, non-detections, or heavily saturated lines.

b Velocity compatible with either a rotating disk or a nuclear outflow.

⁸ Available at http://www.ast.cam.ac.uk/~rfc/vpfit.html.

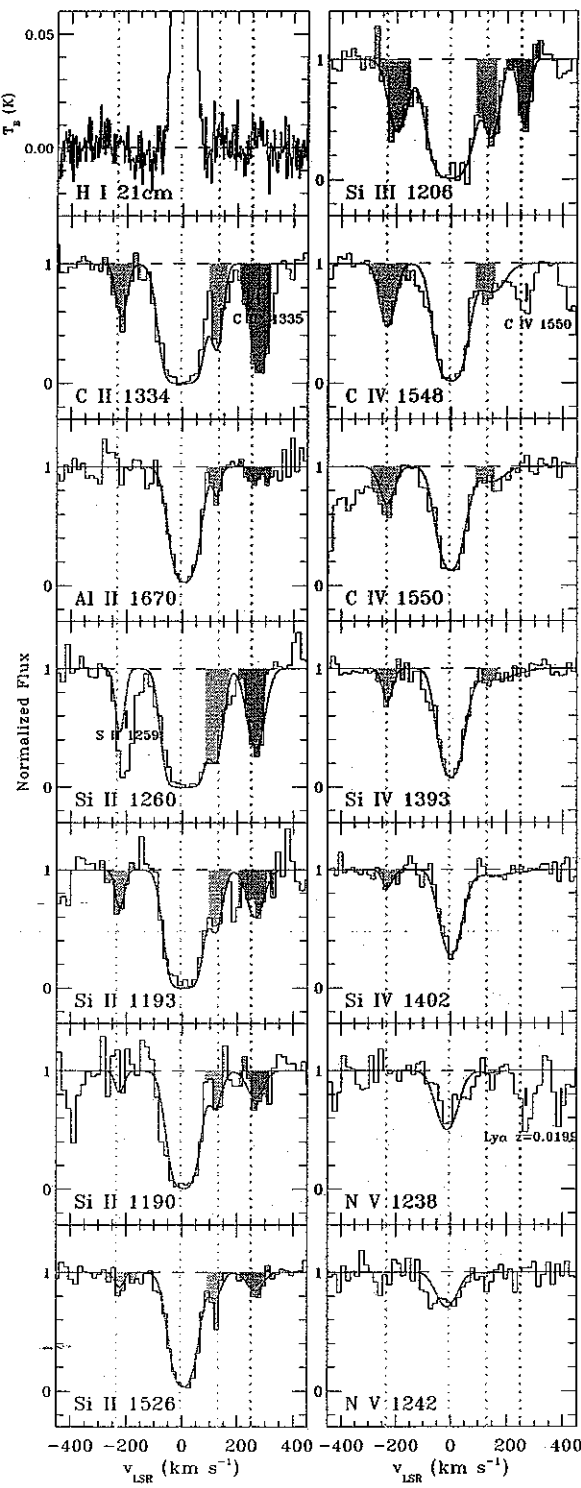


Figure 2. HST/COS and GBT spectra of the quasar PDS 456. Normalized flux is plotted against LSR velocity for all UV metal absorption lines that show high-velocity (HV) absorption (with low ions in the left column and intermediate/high ions in the right column). The GBT H121 cm emission spectrum is included in the top-left panel. Absorption-line components are observed at $v_{\rm LSR}=-235, -5, +130,$ and $+250~{\rm km~s^{-1}}$; only the $-5~{\rm km~s^{-1}}$ component is seen in 21 cm emission. Red lines indicate Voigt-profile fits. The $-5~{\rm km~s^{-1}}$ (unshaded) and $+130~{\rm km~s^{-1}}$ (yellow) components have velocities consistent with co-rotating foreground gas. However, the $-235~{\rm km~s^{-1}}$ (blue) and $+250~{\rm km~s^{-1}}$ (orange) components cannot be explained by co-rotation; instead, their velocities are suggestive of gas swept up by a biconical outflow. In this scenario the near-side of the outflowing cone gives the $-235~{\rm km~s^{-1}}$ component and the far-side gives the $+250~{\rm km~s^{-1}}$ component.

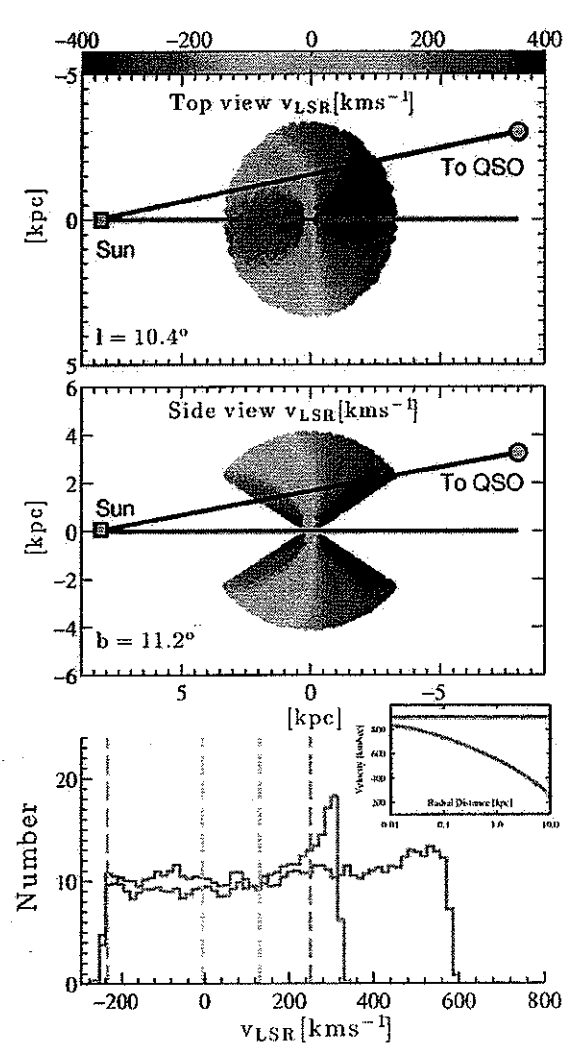


Figure 3. Numerical models of the Galactic biconical nuclear outflow, which can explain the observed absorption-line kinematics. The models have a constant outflow velocity of 900 km s⁻¹ and a full opening angle of 110° (tuned to match the X-ray bicone). We investigate two sets of models: constant-velocity and momentum-driven. Top: top view of the momentum-driven outflow, looking down on the Galactic plane. Each outflow particle is color-coded by its LSR velocity. The near side of the outflow is blueshifted and the far-side of the outflow is redshifted. Middle: side view of the momentum-driven outflow, showing the latitude where the PDS 456 sightline intercepts the bicone. Bottom: distribution of LSR velocities of the outflow particles along the PDS 456 sightline in 100 realizations of the models, for both the constant-velocity (blue line) and momentum-driven (purple line) cases. The inset panel shows the velocity profile of the two models. The centroids of the observed components in the PDS 456 spectrum are shown with vertical lines.

of outflow velocities projected onto the PDS 456 line-of-sight drawn from 100 realizations of each of the two models. Discrete kinematic structure is seen in any single realization of the model (not shown in figure), but the component velocities differ substantially between any two model runs, so we show the distribution to indicate the *range* of velocities predicted.

There are several points to note from the model velocity distributions. First, the distributions are fairly flat for both constant-velocity and momentum-driven winds, which reflects our choice of model in which gas exists with uniform filling factor within the outflow, not just at the edges. The prediction of outflowing gas with LSR velocities near 0 km s⁻¹ could explain the 0.5 dex excess in low-velocity high-ion absorption seen toward

PDS 456. Second, the distributions are asymmetric around zero, ranging from \approx -250 km s⁻¹ (this velocity is a consequence of the requirement that we explain the -235 km s⁻¹ component toward PDS 456) to ≈+550 km s⁻¹ for the constant-velocity wind, and ≈+300 km s⁻¹ for the momentum-driven wind. This asymmetry is a projection effect arising because of the finite distance between the Sun and the GC (the near-field effect). Third, the momentum-driven wind model is more successful in reproducing the range of velocity components seen toward PDS 456 than the constant-velocity wind model, since the latter predicts gas in the range \approx 300–600 km s⁻¹, which is not observed. Models in which gas flows out preferentially along the edges of the cone are also consistent with the data, but are outside the scope of this Letter. In summary, the simple momentum-driven biconical wind model is able to reproduce the velocities of the HV components toward PDS 456.

5. DISCUSSION

The HST/COS spectrum of PDS 456, a QSO lying only 15°.2 from the GC in a direction of enhanced X-ray and γ -ray emission intercepting the base of the northern FB, shows UV metal-absorption-line components at $v_{\rm LSR} = -235$ and $+250\,{\rm km\,s^{-1}}$ (corresponding to $v_{\rm GSR} = -190\,{\rm and}\,+295\,{\rm km\,s^{-1}}$), velocities which cannot be explained by gas in the low halo of the inner Galaxy co-rotating with the disk. A further component at $+130\,{\rm km\,s^{-1}}$ is also difficult to explain via co-rotation. None of the components shows 21 cm emission in our GBT spectrum down to sensitive levels of N (H1) $< 3.3 \times 10^{17}\,{\rm cm^{-2}}\,(3\sigma)$, which indicates the hydrogen is mostly ionized. The kinematics of these components can be explained in a scenario where cool swept-up gas is entrained on the near- (blueshifted) and far- (redshifted) side of a biconical outflow from the GC.

There are several arguments supporting the biconical outflow explanation: (1) the ROSAT X-ray imaging and Fermi y-ray imaging both clearly indicate the presence of a biconical structure centered on the GC and intersected by the PDS 456 sightline, (2) simple kinematic models of a biconical outflow (Section 4) naturally reproduce the presence of both negativeand positive-velocity gas components, (3) such models also explain the excess low-velocity high-ion absorption, (4) the MG13 results demonstrate a population of H_I clumps existing closer to the GC with kinematics consistent with a biconical outflow, (5) although we cannot rule out the possibility that individual HV absorbers arise in unrelated foreground or background HVCs, which have a sky covering fraction in UV metal lines of \approx 68-80% (Collins et al. 2009; Shull et al. 2009; Lehner et al. 2012), a chance alignment of two unrelated HVCs at close-tosymmetric velocities of -235 and +250 km s⁻¹ would be needed to emulate the profiles of a biconical outflow, (6) given the low latitude of the PDS 456 sightline ($b = +11^{\circ}2$), explaining the -235 and +250 km s⁻¹ components as being regular (non-GC) HVCs would require unusually large (≥1000 km s⁻¹) vertical inflow or outflow velocities, because of the projection factor sin b. This makes it highly unlikely that the PDS 456 HV components are due to regular HVCs or to tidally stripped material like the Magellanic Stream, which have much lower vertical flow velocities (\sim 100–200 km s⁻¹).

In the biconical outflow interpretation, the hot wind phase is feeding the FBs with new plasma (e.g., Crocker 2012), whereas the cool low-ion gas represents swept-up material entrained in the outflow. We stress that our HST/COS observations do not directly probe the hot phase, but instead probe cool $(T \sim 10^4 \text{ K})$ entrained gas via the low ions and transition-

temperature ($T \sim 10^5$ K) gas via the high ions, which may trace the boundaries between the cool gas and the hot wind. The cool outflowing gas has already been detected, albeit closer to the GC with a much lower wind velocity, via the MG13 population of H I clouds. Despite the disruptive instabilities that can destroy cold filaments and clouds on short timescales, simulations show that such structures can survive in the hot wind fluid if stabilized by magnetic fields or other mechanisms (Cooper et al. 2008; McCourt et al. 2014).

Our models find the outflow velocity is \gtrsim 900 km s⁻¹; such a flow must be \approx 2.5–4.0 Myr old to reach 2.3 kpc, the impact parameter of the PDS 456 sightline. This wind age is consistent with the timescale of energy injection that created the FBs, whether via AGN jets (Guo & Mathews 2012; Yang et al. 2012), feedback from nuclear star formation (Crocker & Aharonian 2011; Carretti et al. 2013; Lacki 2014), accretion flows onto Sgr A* (Cheng et al. 2011; Mou et al. 2014), or a spherical outflow from Sgr A* (Zubovas et al. 2011). It is also compatible with the observed H α emission from the Magellanic Stream, which is consistent with an origin following a Seyfert flare at the GC 1–3 Myr ago (Bland-Hawthorn et al. 2013).

In our upcoming work, we will analyze the UV spectra of other GC targets, including foreground stars at a range of distance and background AGN at a range of latitude, both inside and outside the FBs. A large sample of sightlines is needed to fully characterize the extent and nature of the Galactic nuclear outflow.

Support for program 13448 was provided by NASA through grants from the Space Telescope Science Institute, which is operated by the Association of Universities for Research in Astronomy, Inc., under NASA contract NAS 5-26555. The National Radio Astronomy Observatory is a facility of the National Science Foundation operated under cooperative agreement by Associated Universities, Inc. We thank Gerald Cecil for assistance with Figure 1 and the referee for an insightful report. We thank Anne Franckowiak and the *Fermi*-LAT collaboration for permission to reproduce their all-sky residual intensity map. J.B.H. is funded by an ARC Laureate Fellowship. T.S.K. acknowledges support from a European Research Council Starting Grant in cosmology and the IGM under Grant Agreement (GA) 257670.

REFERENCES

Ackermann, M., Albert, A., Atwood, W., et al. 2014, ApJ, 793, 64

Bland, J., & Tully, B. 1988, Natur, 334, 43

Bland-Hawthorn, J., & Cohen, M. 2003, ApJ, 582, 246

Bland-Hawthorn, J., Maloney, P. R., Sutherland, R. S., & Madsen, G. J. 2013, ApJ, 778, 58

Boothroyd, A. I., Blagrave, K., Lockman, F. J., et al. 2011, A&A, 536, A81 Bordoloi, R., Lilly, S. J., Kacprzak, G. G., & Churchill, C. W. 2014, ApJ, 784, 108

Bowen, D. V., Jenkins, E. B., Tripp, T. M., et al. 2008, ApJS, 176. 59

Carretti, E., Crocker, R. M., Staveley-Smith, L., et al. 2013, Natur, 493. 66

Cecil, G., Bland-Hawthorn, J., & Veilleux, S. 2002, ApJ, 576, 745

Cecil, G., Bland-Hawthorn, J., Veilleux, S., & Filippenko, A. V. 2001, ApJ, 555, 338

Cheng, K.-S., Chernyshov, D. O., Dogiel, V. A., Ko, C.-M., & lp, W.-H. 2011, ApJ, 731, L17

Collins, J. A., Shull, J. M., & Giroux, M. L. 2009, ApJ, 705, 962

Cooper, J. L., Bickneli, G. V., Sutherland, R. S., & Bland-Hawthorn, J. 2008, ApJ, 674, 157

Crocker, R. M. 2012, MNRAS, 423, 3512

Crocker, R. M., & Aharonian, F. 2011, PhRv1., 106, 101102

Dijkstra, M., & Kramer, R. 2012, MNRAS, 424, 1672

Dobler, G., & Finkbeiner, D. P. 2008, ApJ, 680, 1222

Dobler, G., Finkbeiner, D. P., Cholis, I., Slatyer, T., & Weiner, N. 2010, ApJ, 717, 825

Finkbeiner, D. P. 2004, ApJ, 614, 186

Fox, A. J., Wakker, B. P., Barger, K. A., et al. 2014, ApJ, 787, 147

Green, J. C., Froning, C. S., Osterman, S., et al. 2012, ApJ, 744, 60 Guo, F., & Mathews, W. G. 2012, ApJ, 756, 181

Heckman, T. M. 2002, in ASP Conf. Ser. 254, Extragalactic Gas at Low Redshift, ed. J. S. Mulchaey & J. Stocke (San Francisco, CA: ASP), 292

Kataoka, J., Tahara, N., Totani, T., et al. 2013, ApJ, 779, 57

Keeney, B. A., Danforth, C. W., Stocke, J. T., et al. 2006, ApJ, 646, 951

Lacki, B. C. 2014, MNRAS, 444, L39

Lehner, N., Howk, J. C., Thom, C., et al. 2012, MNRAS, 424, 2896

Lockman, F. J. 1984, ApJ, 283, 90

McClure-Griffiths, N. M., Green, J. A., Hill, A. S., et al. 2013, ApJ, 770. L4, (MG13)

McCourt, M., O'Leary, R. M., Madigan, A.-M., & Quataert, E. 2014, MNRAS, submitted (arXiv:1409.6719)

Mou, G., Yuan, F., Bu, D., Sun, M., & Su, M. 2014, ApJ, 790, 109 Murray, N., Quataert, E., & Thompson, T. A. 2005, ApJ, 618. 569

Ohyama, Y., Taniguchi, Y., Iye, M., et al. 2002, PASJ, 54, 891

Putman, M. E., Peek, J. E. G., & Joung, M. R. 2012, ARA&A, 50, 491 Reid, M. J., Menten, K. M., Zheng, X. W., et al. 2009, ApJ, 700, 137 Ryans, R. S. I., Dufton, P. L., Keenan, F. P., et al. 1997, ApJ, 490, 267

Savage, B. D., & Massa, D. 1987, ApJ, 314, 380

Savage, B. D., Meade, M. R., & Sembach, K. R. 2001, ApJS, 136, 631

Savage, B. D., Sembach, K., & Massa, D. 1990, ApJ, 355, 114

Sembach, K. R., Savage, B. D., & Massa, D. 1991, ApJ, 372, 81

Shopbell, P. L., & Bland-Hawthorn, J. 1998, ApJ, 493, 129

Shull, J. M., Jones, J. R., Danforth, C. W., & Collins, J. A. 2009, ApJ, 699. 754

Snowden, S., Egger, R., Freyberg, M., et al. 1997, ApJ, 485, 125 Su, M., Slatyer, T. R., & Finkbeiner, D. P. 2010, ApJ, 724, 1044

Veilleux, S., Cecil, G., & Bland-Hawthorn, J. 2005, ARA&A, 43, 769

Veilleux, S., & Rupke, D. 2002, ApJL, 565, L63

Wakker, B. P., Savage, B. D., Fox, A. J., Benjamin, R. A., & Shapiro, P. R. 2012, ApJ, 749, 157

Yang, H.-Y. K., Ruszkowski, M., Ricker, P. M., Zweibel, E., & Lee, D. 2012, ApJ, 761, 185

Zech, W. F., Lehner, N., Howk, J. C., Dixon, W. V. D., & Brown, T. M. 2008, ApJ, 679, 460

Zubovas, K., King, A. R., & Nayakshin, S. 2011, MNRAS, 415, L21